Solid Freeform Fabrication 2024: Proceedings of the 35th Annual International Solid Freeform Fabrication Symposium – An Additive Manufacturing Conference
Reviewed Paper

Defect-free Ceramic Hybrid-AM using Intelligent Layer Reworking

L. Masters*, T. Green*, D. Davie*, M. P. Shuttleworth*, M. Dogar†, and R. W. Kay*

*School of Mechanical Engineering, University of Leeds, United Kingdom, LS2 9JT
†School of Computing, University of Leeds, United Kingdom, LS2 9JT

Abstract

Hybrid additive manufacturing of advanced ceramics facilitates the production of highly dense and precise parts by combining additive and subtractive processes. However, extrusion-based processes are susceptible to stochastic defects such as voids, or under extrusions, which can degrade material properties, leading to premature failure and lower yield. This research demonstrates deep learning informed selective layer reworking for a ceramic hybrid additive manufacturing platform. Each layer was evaluated in-situ using a vision-based monitoring system, consisting of a camera and a laser profilometer. Through closed-loop control, a decision was made autonomously to pause production, allowing for defect repair prior to reprinting the layer. The deep learning model detected voids with a precision of 90%, and the laser algorithm achieved F scores greater than 98% across a range of parts, facilitating future corrective actions to repair these regions. This unlocks new opportunities for regulated industries aiming to exploit quality-assured ceramic components that benefit from freeform fabrication.

Introduction

Hybrid additive manufacturing (Hybrid-AM) systems are becoming increasingly popular in both research and industrial settings, as the combination of multiple processes, particularly additive and subtractive, creates new manufacturing opportunities [1–3]. Integrating multiple processes into a singular machine offers several advantages including: higher levels of autonomy, multi-material or functionally graded parts, improved part quality, and shorter cycle times [3–5]. Hybrid-AM has been used successfully for metals, ceramics, and polymers. As the technology is still emerging, there is need for improved software packages to utilize the true potential of these machines; most existing software for Hybrid systems consists of bespoke, application specific toolpath generation software [5,6]. The software control offering for these machines is based on existing CNC/3D printing motion controllers, which does not support new operations being generated on the fly based on process feedback. To encourage further academic and industry adoption of Hybrid-AM, the software control of these machines, in particular sensor-driven feedback, must be improved.

In-situ monitoring of extrusion AM processes has been explored significantly in existing research, with a variety of different sensing methods [7–11]. Extrusion-based AM processes are vulnerable to process defects [12], which can cause parts to fail mid-production, or lead to premature failure during use. Underextrusions, or voids, are particularly problematic as they influence the final properties of a part [13,14]. However, the majority of this work primarily concerns detecting defects, with few opting to extend the issue to defect repair [15,16]. While this is largely down to a standard 3D printer being limited to only deposit material, with the emergence of hybrid-AM systems new corrective measures can be explored for defect-free manufacturing. Additionally, multi-modal sensing is becoming more common, allowing for a greater

understanding of processes. Multi-modal sensing, can be used to alleviate the disadvantages of individual sensors, allowing for a wider selection of defect types or process instabilities to be monitored. For example, vision-based defect detection is unable to detect internal voids, or capture 3D measurements, but when combined with a measurement systems like acoustic monitoring or laser triangulation, more detailed evaluations of part integrity can be generated.

Methodology

Manufacturing Apparatus

The manufacturing system used in this work was a Ceramic Hybrid Additive Manufacturing Platform (CHAMP). The CHAMP combined a high viscosity ceramic paste extruder, machining spindle with automatic tool changer, IR drying lamp and an in-situ, multi-modal sensing system.

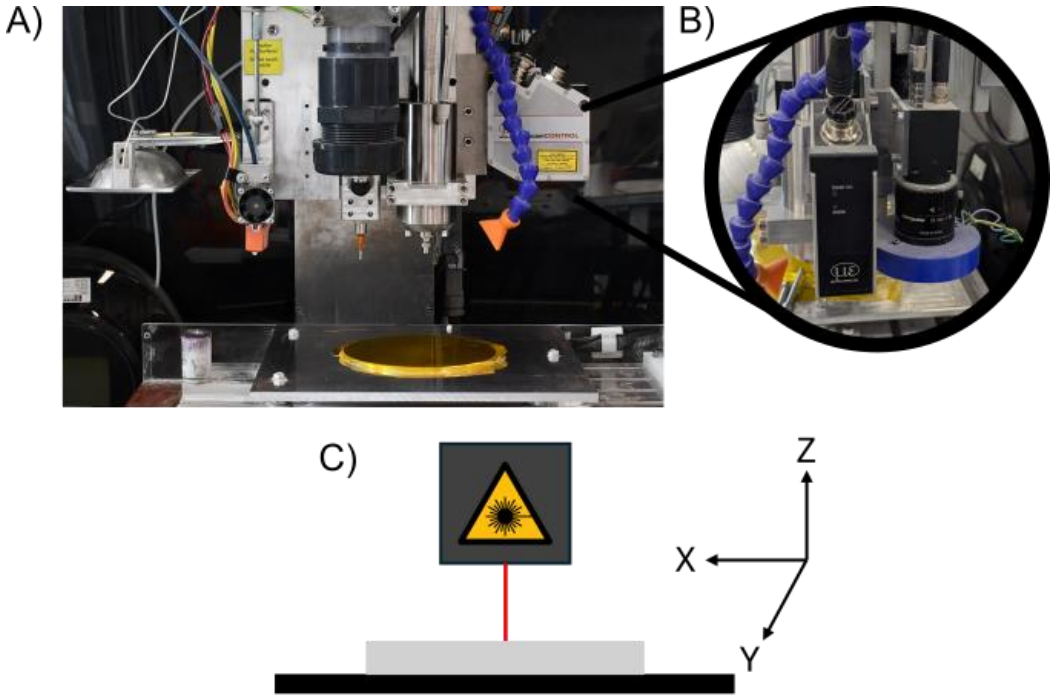

Figure 1: A) Overview of the CHAMP, B) the in-situ measurement system, C) the laser coordinate system

The multi-modal sensing system uses a high-resolution camera and a laser profilometer to record part data. Multi-modal sensing incorporates two or more sensors to generate more data about a process. The proposed method was a two-step monitoring process; first the camera captured images of each layer, and a deep learning model was used to determine if the layer contained any under or over extrusions. If the layer contained under extrusions, the entire layer was considered defective and would require repair. In the case where only over extrusions were detected, and were large relative to the part size, a laser scan was carried out. A point-cloud was generated, and compared to a point-cloud generated from the gcode file to determine the significance of the over extrusion, and when required a correction was performed. The YOLO model provided fast detection of voids, but the laser system was introduced because the model could not quantify the scale of the over extrusions in the Z direction. Over extrusions that deviated from the intended layer height significantly were more influential on subsequent layer quality than over extrusions with a

lesser Z deviation but greater X, Y area, based on operator experience. This was due to the nozzle being dragged through the surplus material, which stuck to the nozzle and can foul non-defective regions.

The measurement system consisted of a monochrome camera (VCXU.2-201M.R, Baumer Vision Technologies) with a telephoto lens (V1226-MPZ, Computar), and a laser profilometer (scanCONTROL 2900-50, MicroEpsilon). The camera sensor pixel size was 2.4µm and the image resolution was 5472x3648px. The laser scanner was positioned 70 mm from the build plate, giving a resolution of 0.045 mm and 0.004 mm in the Y and Z direction, respectively. In the X direction, scans were captured in 0.5 mm intervals. The acquisition of both camera and laser data was controlled by a bespoke process monitoring script written in Python.

YOLO Model

A You-Only-Look-Once (YOLO) [17] v8 small model was used in this work, a high-level network architecture is shown in Fig 2. The YOLO model was selected as it is one of the best performing models for object detection both in terms of accuracy and inference speed. A small model was chosen to limit inference time and reduce the computational requirements for training. The model was trained on the COCO dataset [18] before being trained on a bespoke data set consisting of 432 images containing 3289 under extrusions and 3125 over extrusions. The data was labelled using bounding boxes by an operator familiar with the process, and contained naturally occurring defects, forced defects and non-defective images. This was divided using a 70:20:10 split into training, validation, and test images. The remaining 300 training images underwent data augmentation to increase the variation in the data and the number of images. The following augmentations were applied: horizontal and vertical flips (P=0.5), rotation ±45˚ (P=Rand), brightness adjustment ±25% (P=Rand), gaussian blur 0-2.5px (P=Rand) and 2% noise. This

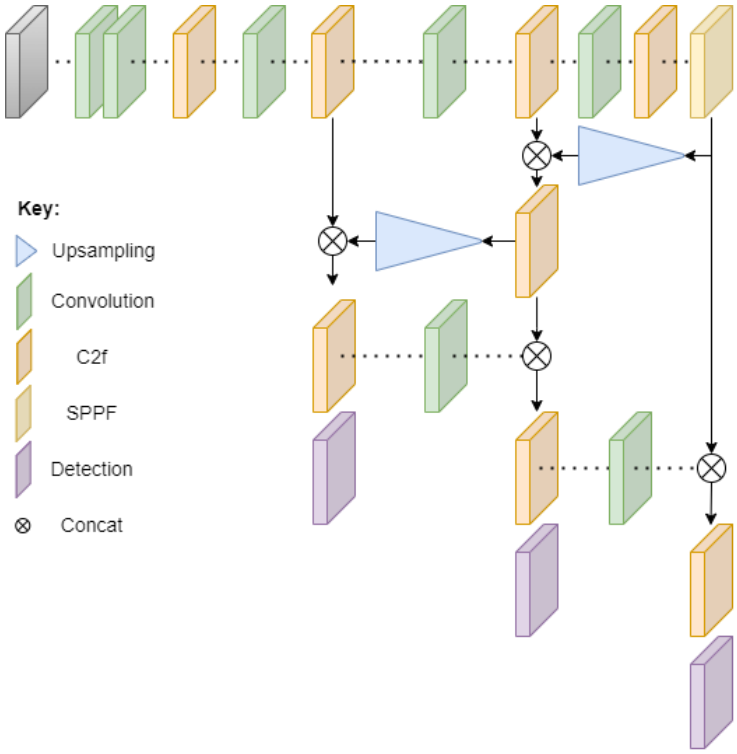

Figure 2: High-level overview of the YOLOv8 network architecture

increased the training set to 3000 images. Finally, the images were downsized to 2048x1365 to reduce the computational cost of training. The YOLO model was trained using PyTorch and the Ultralytics python packages. This work was undertaken on ARC4, part of the High Performance Computing facilities at the University of Leeds, UK. A single node of the ARC4 cluster was used, consisting of an Intel Xeon Gold 6138 CPU, four Nvidia Tesla V100 GPUs, and 192Gb of RAM. Two GPUs were required during training due to the high-resolution images.

The model was trained for 300 epochs using a batch size of 8, and an Intersection-over-Union, (IoU) threshold of 0.7, which is the required overlap between predictions and ground truth labels to count as positive prediction. All other variables were left as their default values stated in the Ultralytics package. In training, multiple metrics were used to evaluate the performance of the model using the validation dataset, and after training the unseen test data was used to determine how well the model had generalized. These metrics were as follows:

- Precision, P – The ratio of true positives to all positives = TP/(TP + FP).
- Recall, R – The ratio of true positives to class instances = TP/(TP+FN).
- Mean Average Precision, mAP – The mean of the average precision, area under P-R curve.
- F1-score, F_1 – The harmonic mean between precision and recall.

Where TP= True Positive, FP= False Positive and FN = False Negative. Two different mAP metrics were calculated, mAP@50 = the mAP at the 0.5 IoU thresholds, and mAP@50-95 = the mAP at a range of IoU thresholds between 50-95%.

Laser Measurement system

The Laser Measurement system was introduced to evaluate over extrusions. Measurements were taken when the YOLO model detected solely over extrusions. A flowchart outlining the combined monitoring procedure is given in Figure 3. Once a scan was captured, the data was filtered to remove any non-numeric values or erroneous points that appeared below the build plate resulting from the occlusion of the laser. Simultaneously, the python script processed the gcode of the part, creating a series of polygons representing the outline of the part geometry, including external perimeters or internal features such as holes. Polygons were stored as point clouds (PCs) and passed through a multiple polygon filtering (MPF) algorithm to extract definitive inlier points. This novel algorithm operated on two base principles:

1. A polygon representing a hole had an area less than the polygon representing the outline of the material surrounding it.
2. The area in-between two nested polygons alternate between a hole (outlier) or an extrusion (inlier).

However, gcode coordinates refer the centerpoint of an extruded raster, meaning the outer part of the extrudates were absent from the MPF algorithm. This was addressed by extracting all remaining points greater than a lower limit, which was calculated by:

$$Lower\ Limit = \mu_i - \sigma_i \times SD_{multi}$$

where μ_i = inlier point cloud mean, σ_i = inlier standard deviation and SD_{multi} = standard deviation multiplier. This correction enabled the algorithm to dynamically adjust the acceptable deviation of additional points depending on the variation measured in the print, ensuring the lowest number of points to attain a good layer representation were extracted. These additional points were combined

with the inlier points previously extracted. During testing, two further checks were implemented to the lower limit calculation:

1. A minimum deviation value was set at 0.2mm, one third of a layer height. This ensured the algorithm would always extract some number of points irrespective of layer quality.
2. A grounding value was introduced to prevent the algorithm extracting previous layers or build plate points. This was achieved by expanding the gcode polygon to remove points representing an extrusion, leaving only points on the build plate. A grounding value of 0.15mm was selected, which fell within the build plate PCs deviation, and enabled severe under extrusions to be extracted.

$$range = minimum\ deviation + (standard\ deviation\ \times multiplier)$$

$$Lower\ Limit = \begin{cases} grounding\ value, & \text{if } range < grounding\ value \\ range, & \text{otherwise.} \end{cases}$$

Once PCs were created, they were segmented into over and under extrusions based on the mean point cloud height, and Euclidean clustering was applied to group points into defect regions. From this the area and height deviation of defective clusters were calculated. The laser and point cloud clustering algorithm was evaluated by printing intentionally under extruded and over extruded tiles, as well as unaltered bracket part. An ideal PC was manually created for each layer to obtain all defect regions and serve as a ground-truth to compare the algorithm to. An F-score was calculated from the difference between the ground truth and algorithm results. An F-score is the harmonic mean of precision and recall, and is a statistical measure of predictive performance, a score of 1 indicating perfect performance.

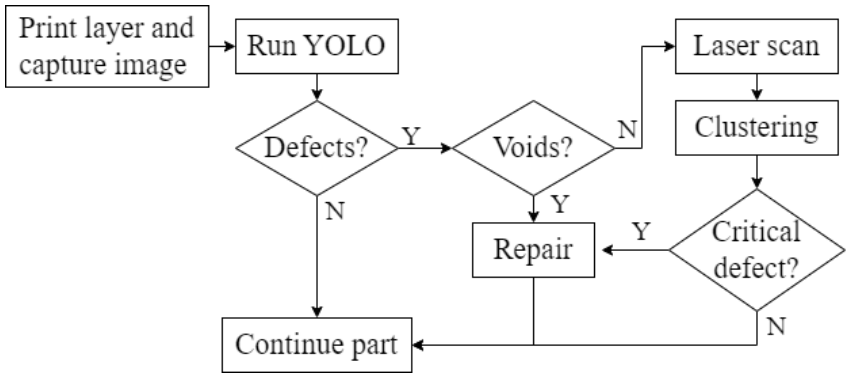

Figure 3: Flowchart outline of the combined in-situ monitoring process

The proposed repair processes were simple; if a layer contains voids, it is defective and must be removed and reprinted. If a layer contains solely over extrusions that were deemed significant, then that layer would be planarized prior to depositing a subsequent layer to remove excess material that may interfere with additional layers.

Results and discussion

YOLO Model

The results from the YOLO model against unseen test data are given in Table 1. The model performed well on the under extrusion class, achieving a precision of 89.5%. However, the performance at detecting over extrusions was worse against all metrics, further highlighted in the F1-Confidence Curve in Figure 4. The maximum F1 score of 0.75 was achieved at a confidence level of 0.425, and the curve shows that the detection of under extrusions is better across a range of confidence thresholds. Under extrusions impact the properties of final parts and can also lead to a print failing. Over extrusions are not always significant, but multiple instances in one layer, or significant Z deviation can cause issues printing subsequent layers. The models lower performance against over extrusions likely stems from both a labelling inconsistency in the training data, and the low contrast between over extrusion locations and the rest of the part. When labelling the data, it was difficult to determine when small debris should be considered an over extrusion or ignored. The false positive predictions stemming from this inconsistency were penalized during training, reducing performance on this defect class. In the case of large over extrusions there was a small shadow cast on the rest of the part, increasing contrast, which was included within the labelled region. Smaller over extrusions were less pronounced, cast no shadows and therefore had lower contrast. Combined with the expected texture of the layers, this posed challenges during data labelling and subsequent training of the network.

Table 1: Results of the YOLOv8s model on unseen test data.

Defect class	mAP@50-95	mAP@50	Precision	Recall
Both classes	0.4520	0.7808	0.8055	0.7039
Under extrusion	0.4879	0.8452	0.8953	0.7241
Over extrusion	0.4160	0.7164	0.7156	0.6837

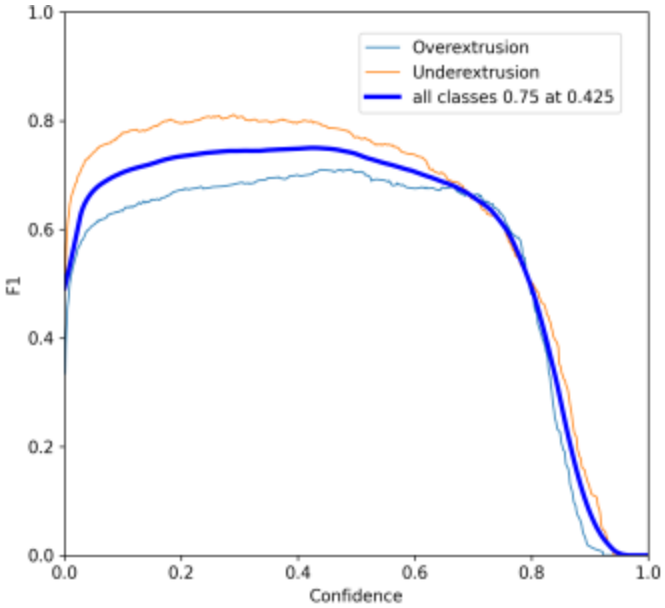

Figure 4: F1-Confidence Curve, indicating the optimum performance at confidence level 0.425

This could be addressed by increasing the amount of training data to average out these inconsistencies. An emphasis should be placed on increasing the number of over extrusion

examples, as well as samples with no defects, so that the model might better distinguish between acceptable surface texture and defects. However, generating and processing this data is time consuming; alternatively, the laser measurement system could be used to evaluate the severity of over extrusion defects and determine if a correction is required.

Laser system

The results of the laser and PC clustering algorithms performance of the 3 parts for a range of standard deviation multipliers are given in Table 2. The standard deviation multiplier was increased in 0.5 intervals from 0.5 to 2. In this coarse study, the algorithm demonstrated excellent performance on all 3 parts, figure 5. The high F-scores across the range of standard deviation multipliers indicate the extraction algorithm is effectively extracting layer geometry information regardless of layer quality. Existing point cloud extraction algorithms are typically demonstrated on layers from the middle of the part, likely due to difficulties encountered separating the features from the build plate. We demonstrate here an approach that works effectively irrespective of layer number and quality.

Table 2:Performance of the extraction algorithm across a range of standard deviation multipliers.

SD_{multi}	F-score		
	Under extruded	**Bracket**	**Over extruded**
0.5	0.9961	0.9992	0.9834
1.0	0.9961	0.9997	0.9873
1.5	0.9961	0.9999	0.9907
2.0	0.9961	1.0000	0.9957
2.5	0.9961	0.9999	0.9980

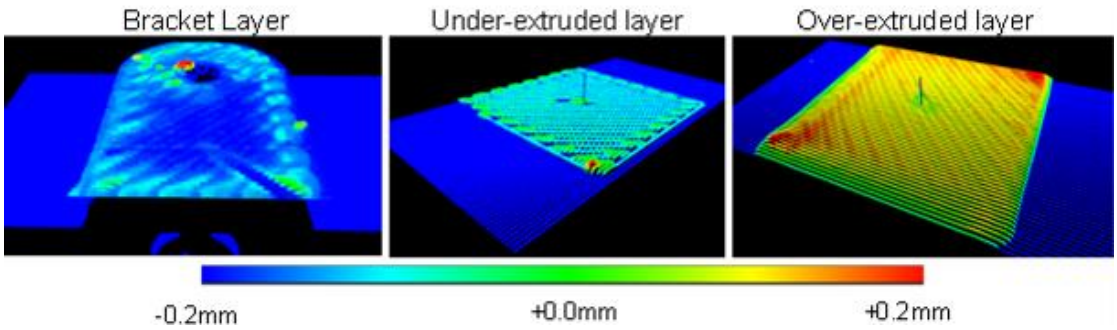

Figure 5: Visualization of the algorithm's deviation calculation across the three parts

As the algorithm effectively clustered defective regions, and calculated defect area and Z deviation, it could be used to support the results of the YOLO model. For example, the model could detect an over extrusion across the entire surface of the part. Due to the size of this detection, a laser measurement is undertaken. The laser measurement determines that the Z deviation is small, and therefore the defect is unlikely to affect subsequent layers. Whilst the time taken to confirm this with the laser scan is longer than solely the YOLO model, it would alleviate an unnecessary corrective operation, improving overall process efficiency.

Conclusions

In-situ monitoring has become a significant feature of many modern manufacturing processes, aiding in process optimization to create better products with fewer defects. With high

quality sensors becoming widely available, multi-modal sensing has become increasingly common, offering a higher level of machine intelligence and a more comprehensive evaluation of process defects.

This work presents preliminary research into a vision-based deep learning system for identifying defects in ceramic parts. This system identified under extrusions with around 90% precision, but performed worse on over extrusions, and so an additional sensing method in the form of a laser scanner was introduced. This laser data provided a 3D evaluation of the layer quality to support the detection from the YOLO model before a decision on repair was made. The clustering algorithm reliably segmented deviated regions, with a minimum F-score of 0.98 across the 3 case studies. This would ensure that an operator would not be instructed to repair over extrusions that were unlikely to lead to further defects, improving manufacturing efficiency.

As this work was incorporated into a hybrid manufacturing system, there exists the possibility to add and remove material. Future work will focus on establishing a feedback loop between the monitoring system and the manufacturing platform. Using this feedback loop, with improved toolpath generation, there is an opportunity to repair the defects mid-process. This would highlight the full potential of hybrid manufacturing combined with multi-modal sensing for the creation of high-value, defect-free parts.

References

[1] B. Nau, A. Roderburg, F. Klocke, Ramp-up of hybrid manufacturing technologies, CIRP J Manuf Sci Technol 4 (2011) 313–316. https://doi.org/10.1016/J.CIRPJ.2011.04.003.

[2] T. Feldhausen, K. Saleeby, T. Kurfess, Spinning the digital thread with hybrid manufacturing, Manuf Lett 29 (2021) 15–18. https://doi.org/10.1016/J.MFGLET.2021.05.003.

[3] P. Stavropoulos, H. Bikas, O. Avram, A. Valente, G. Chryssolouris, Hybrid subtractive-additive manufacturing processes for high value-added metal components. https://doi.org/10.1007/s00170-020-06099-8/Published.

[4] K.A. Lorenz, J.B. Jones, D.I. Wimpenny, M.R. Jackson, A Review of Hybrid Manufacturing, 2014 International Solid Freeform Fabrication Symposium, University of Texas at Austin, 2015. https://repositories.lib.utexas.edu/handle/2152/89311.

[5] J.M. Flynn, A. Shokrani, S.T. Newman, V. Dhokia, Hybrid additive and subtractive machine tools – Research and industrial developments, Int J Mach Tools Manuf 101 (2016) 79–101. https://doi.org/10.1016/J.IJMACHTOOLS.2015.11.007.

[6] Z. Zhu, V. Dhokia, S.T. Newman, A. Nassehi, Application of a hybrid process for high precision manufacture of difficult to machine prismatic parts, https://doi.org/10.1007/s00170-014-6053-7.

[7] A.L. Petsiuk, J.M. Pearce, Open source computer vision-based layer-wise 3D printing analysis, Addit Manuf 36 (2020) 101473. https://doi.org/10.1016/J.ADDMA.2020.101473.

[8] T. Fang, M.A. Jafari, S.C. Danforth, A. Safari, Signature analysis and defect detection in layered manufacturing of ceramic sensors and actuators, (2003). https://doi.org/10.1007/s00138-002-0074-1.

[9] Y. Chen, X. Peng, L. Kong, G. Dong, A. Remani, R. Leach, Defect inspection technologies for additive manufacturing, International Journal of Extreme Manufacturing 3 (2021) 022002. https://doi.org/10.1088/2631-7990/abe0d0.

[10] Y. Jiang, H. Wang, G. Tian, S. Chen, L. Zhang, Visual Detection of AM Surface Defects Based on Laser Ultrasound Technology, Proceedings of 2019 IEEE Far East NDT New Technology and Application Forum, FENDT 2019 (2019) 6–10. https://doi.org/10.1109/FENDT47723.2019.8962808.

[11] P. Charalampous, I. Kostavelis, C. Kopsacheilis, D. Tzovaras, Vision-based real-time monitoring of extrusion additive manufacturing processes for automatic manufacturing error detection, International Journal of Advanced Manufacturing Technology 115 (2021) 3859–3872. https://doi.org/10.1007/S00170-021-07419-2/FIGURES/12.
[12] Y. Tao, F. Kong, Z. Li, J. Zhang, X. Zhao, Q. Yin, D. Xing, P. Li, A review on voids of 3D printed parts by fused filament fabrication, Journal of Materials Research and Technology 15 (2021) 4860–4879. https://doi.org/10.1016/J.JMRT.2021.10.108.
[13] N. Sato, K. Takahashi, Evaluation of Fracture Strength of Ceramics Containing Small Surface Defects Introduced by Focused Ion Beam, Materials 11 (2018). https://doi.org/10.3390/MA11030457.
[14] K. Ando, B.A. Kim, M. Iwasa, N. Ogura, Process zone size failure criterion and probabilistic fracture assessment curves for ceramics, Fatigue Fract Eng Mater Struct 15 (1992) 139–149. https://doi.org/10.1111/J.1460-2695.1992.TB00044.X.
[15] D.A.J. Brion, M. Shen, S.W. Pattinson, Automated recognition and correction of warp deformation in extrusion additive manufacturing, Addit Manuf 56 (2022) 102838. https://doi.org/10.1016/J.ADDMA.2022.102838.
[16] D.A.J. Brion, S.W. Pattinson, Generalisable 3D printing error detection and correction via multi-head neural networks, Nature Communications 2022 13:1 13 (2022) 1–14. https://doi.org/10.1038/s41467-022-31985-y.
[17] J.S.D.R.G.A.F. Redmon, You Only Look Once: Unified, Real-Time Object Detection, Conference on Computer Vision and Pattern Recognition (CVPR) 2016-December (2016) 779–788. https://doi.org/10.1109/CVPR.2016.91.
[18] T.-Y. Lin, M. Maire, S. Belongie, L. Bourdev, R. Girshick, J. Hays, P. Perona, D. Ramanan, C.L. Zitnick, P. Dolí, Microsoft COCO: Common Objects in Context.